Phys. Status Solidi C **13**, No. 10–12, 913–920 (2016) / **DOI** 10.1002/pssc.201600074

physica status solidi c
www.pss-c.com
current topics in solid state physics

Ab initio calculations of $PbTiO_3/SrTiO_3$ (001) heterostructures

R. I. Eglitis[*], S. Piskunov[**], and Yu. F. Zhukovskii[***]

Institute of Solid State Physics, University of Latvia, 8 Kengaraga Str., 1063 Riga, Latvia

Received 27 May 2016, revised 3 July 2016, accepted 15 July 2016
Published online 9 August 2016

Keywords *ab initio* calculations, $PbTiO_3/SrTiO_3$, (001) heterostructures, band gap, B3PW hybrid functional

* Corresponding author: e-mail rieglitis@gmail.com, Phone: +371-26426703, Fax: +371-67132778
** e-mail piskunov@lu.lv, Phone: +371-20093610, Fax: +371-67132778
*** e-mail quantzh@latnet.lv, Phone: +371-28824271, Fax: +371-67132778

We performed *ab initio* calculations for the $PbTiO_3/SrTiO_3$ (001) heterostructures. For both PbO and TiO_2-terminations of the $PbTiO_3$ (001) thin film, augmented on the $SrTiO_3$ (001) substrate, the magnitudes of atomic relaxations Δz increases as a function of the number of augmented monolayers. For both terminations of the augmented $PbTiO_3$ (001) nanothin film, all upper, third and fifth monolayers are displaced inwards (Δz is negative), whereas all second, fourth and sixth monolayers are displaced outwards (Δz is positive). The B3PW calculated $PbTiO_3/SrTiO_3$ (001) heterostructure band gaps, independently from the number of augmented layers, are always smaller than the $PbTiO_3$ and $SrTiO_3$ bulk band gaps. For both PbO and TiO_2-terminated $PbTiO_3/SrTiO_3$ (001) heterostructures, their band gaps are reduced due to the increased number of $PbTiO_3$ (001) monolayers. The band gaps of PbO-terminated augmented $PbTiO_3$ (001) films are always larger than those for TiO_2-terminated $PbTiO_3$ (001) thin films. The only exception is the case of 7-layer PbO-terminated and 8-layer TiO_2-terminated augmented $PbTiO_3$ (001) thin films, where their band gaps both are equal to 2.99 eV. For each monolayer of the $SrTiO_3$ (001) substrate, charge magnitudes always are more than several times larger, than for each monolayer in the augmented $PbTiO_3$ (001) thin film.

1 Introduction During the last several years emerging new and forefront technologies make it possible to grow $PbTiO_3/SrTiO_3$ (001) superlattices and ultrathin films with atomic control. Practically all nanoscale devices possess metal-dielectric, metal-semiconductor, semiconductor-semiconductor, or semiconductor-ferroelectric interfaces. Therefore, the investigation of complex oxide interfaces is a very important research area due to the current and forthcoming huge number of nanoscale device applications. Surface and interface phenomena and their nanostructures, the nature of surface and interface states, the mechanisms of surface electronic processes are all very important topics in modern solid state physics [1-9]. Despite the great industrial potential of $SrTiO_3$ and $PbTiO_3$ perovskites, as well as large number of first principles calculations dealing with their pristine (001) surfaces [10-30], it is rather difficult to understand the reason, why up to now only a small number of experimental and *ab initio* investigations are performed dealing with $PbTiO_3/SrTiO_3$ (001) heterostructures [31-38].

$SrTiO_3$ probably is technologically most important ABO_3 perovskite. Pristine $SrTiO_3$ (001) thin films are used for a huge number of industrial applications, such as, for example, substrates for high-T_C cuprate superconductor growth, catalysis, integrated optics, optical wave guides, as well as high capacity memory cells [39]. From the fundamental point of view $SrTiO_3$ is so called incipient ferroelectric. At room and higher temperatures $SrTiO_3$ is a centrosymmetric paraelectric ABO_3 perovskite material in a cubic high symmetry $Pm3m$ phase. As temperature lowers, $SrTiO_3$ approaches a ferroelectric phase transition with a very large dielectric constant ~10^4, however, it remains paraelectric down to the lowest measured temperatures. $PbTiO_3$ (001) surfaces have significant advantages in reducing the weight and size of electronic devices, which have important applications in microelectronics, such as, for example, multilayer capacitors, infrared pyroelectronic sensors, non-volatile memories, and ultrasonic transducers [40]. Regarding the atomic structure $PbTiO_3$ is paraelectric (nonpolar) at high temperatures and have the cubic

perovskite structure with space group *Pm*3*m*. In contrast to incipient ferroelectric $SrTiO_3$, as temperature lowers, $PbTiO_3$ has one cubic to tetragonal phase transition at 766 K [41]. In order to keep our calculation time realistic, we performed all our calculations only for high symmetry cubic phases of $SrTiO_3$ and $PbTiO_3$ perovskites. These two materials in the cubic phase co-exist only at temperatures above 766 K.

In this paper, we present results of our *ab initio* calculations on atomic and electronic structure of technologically important $PbTiO_3/SrTiO_3$ (001) heterostructures using $SrTiO_3$ (001) surface as a substrate for $PbTiO_3$ growth. The paper is organized as follows. The computational details of our numerical calculations are described in Section 2. Section 3 presents results of our *ab initio* calculations on $PbTiO_3/SrTiO_3$ (001) heterostructures, including the electronic charge redistribution and band structure peculiarities as a function from the number of interface layers and termination type. Finally, our conclusions are systematized in Section 4.

It is worth to notice, that according to our predictions, $PbTiO_3/SrTiO_3$ (001) heterostructures with even number of layers inside $PbTiO_3$ nanothin films (stoichiometric configurations) can be directly suitable for photocatalytic applications after their doping by non-metal atoms substituted regular oxygens (e.g., N_O and S_O mono-dopants as well as N_O+S_O co-dopant).

2 Computational details of the $PbTiO_3/SrTiO_3$ (001) heterostructure calculations We have performed *ab initio* DFT-B3PW numerical calculations for the $PbTiO_3/SrTiO_3$ (001) heterostructures using the periodic *CRYSTAL09* computer code [42]. In contrast to the plane wave codes, the *CRYSTAL* computer code utilizes the Gaussian-type functions centered on atomic nuclei as the basis sets (BSs). The BSs are believed to be completely transferable, so that, once determined for some chemical constituent, they are always applied in the calculations for a variety of materials where the former is included. Such BSs for all chemical elements Pb, Sr, Ti and O of $PbTiO_3$ and $SrTiO_3$ ternary oxides were developed more than a decade ago by Piskunov et al. [43]. Of course, we used exactly the same basis set [43] in our current $PbTiO_3/SrTiO_3$ (001) heterostructure calculations.

In our numerical calculations the hybrid B3PW exchange-correlation functional [44] is employed, increasingly popular in solid state physics during the last decade. The main advantage of this functional is improved description of the experimental band gap in comparison with pure DFT based methods [29, 43]. For description of effective atomic charges on atoms, as well as bond populations between atoms, we have used the classical Mulliken bond population analysis as described in Refs. [45-48]. We performed the reciprocal space integration in our calculations by sampling $PbTiO_3/SrTiO_3$ (001) heterostructure Brillouin zone with the 8 × 8 × 1 Monkhorst-Pack mesh [49].

Since $SrTiO_3$ is an incipient ferroelectric, the $SrTiO_3$ substrate always has high symmetry cubic *Pm*3*m* phase. In order to make our calculations feasible, also $PbTiO_3$ has been calculated as perfect cubic structure. All calculations on $PbTiO_3/SrTiO_3$ (001) heterostructures were performed for their single slab model. All slabs employed in our calculations have been symmetrically terminated in order to maximally use the 2D symmetry. For a substrate we have used symmetrical (with respect to the mirror plane) $SrTiO_3$ (001) slab consisting of eleven alternating TiO_2 and SrO layers (TiO_2-SrO-TiO_2-SrO-TiO_2-SrO-TiO_2-SrO-TiO_2-SrO-TiO_2). Thereby, in our B3PW calculations, the $SrTiO_3$ (001) substrate consisted of a supercell containing 28 atoms. The $SrTiO_3$ (001) substrate is non-stoichiometric, consisting of $Sr_5Ti_6O_{17}$ formula units *per* cell. As a next step in our calculations, we symmetrically and gradually augmented from one to ten alternating PbO and TiO_2 layers (PbO-TiO_2-PbO-TiO_2-PbO-TiO_2-PbO-TiO_2-PbO-TiO_2) on both sides of the $SrTiO_3$ (001) substrate. Thereby, the complete $PbTiO_3/SrTiO_3$ (001) heterostructure in our calculations contains $SrTiO_3$ (001) substrate, consisting of eleven layers, or 28 atoms, and ten $PbTiO_3$ (001) layers containing 25 atoms, augmented symmetrically from both sides of the substrate. The largest number of atoms, in our $PbTiO_3/SrTiO_3$ (001) heterostructure calculations achieves 78 atoms, with unit cell formula $Sr_5Pb_{10}Ti_{16}O_{47}$ (Fig. 1). In B3PW $PbTiO_3/SrTiO_3$ (001) heterostructure calculations coordinates of all system atoms were allowed to relax, but only along the *z*-axis, due to symmetry constraints.

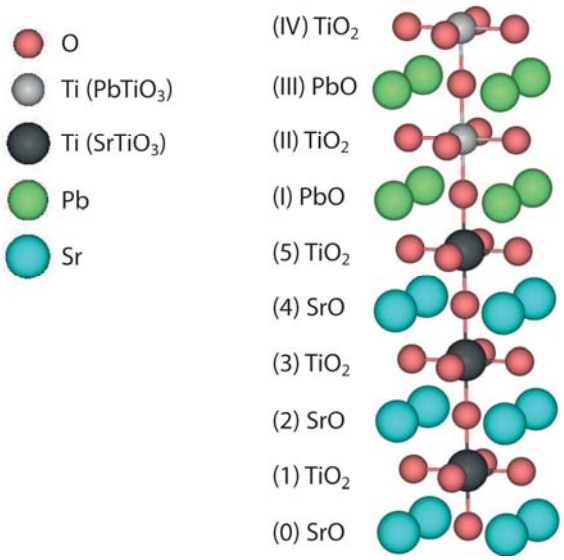

Figure 1 Sketch of the (001) interface between two perovskites $PbTiO_3$ and $SrTiO_3$. Substrate $SrTiO_3$ (001) planes are numbered with Arabic numbers. We used Roman numbers in order to number planes of deposited $PbTiO_3$ (001) film. Arabic number zero is used for the central plane of the symmetrically terminated eleven-layer $SrTiO_3$ (001) substrate.

During epitaxial $PbTiO_3$ film growth, the lattice mismatch between $PbTiO_3$ and $SrTiO_3$ lattice constants arises. Therefore, in B3PW calculations, we performed the relaxation of joint $PbTiO_3/SrTiO_3$ (001) heterostructure lattice constant for the case of thickest $PbTiO_3/SrTiO_3$ (001) heterostructure, consisting of 31 layers and containing 78 atoms, in order to minimize the strain effect. Then, this joint lattice constant 3.91 Å is used in all further numerical $PbTiO_3/SrTiO_3$ (001) heterostructure calculations. To calculate the displacement Δz for each monolayer inside $PbTiO_3/SrTiO_3$ (001) heterostructure, we used the displacement of the previous atomic monolayer. Thereby, the reference z-coordinate for each monolayer N is described using the following equation:

$$z_N^{ref} = \tfrac{1}{2}\left(z_{N-1}^{Me} + z_{N-1}^{O}\right), \quad (1)$$

where z_{N-1}^{Me} and z_{N-1}^{O} are the z-coordinates of the metal atom and oxygen atom of the previous atomic monolayer, respectively.

3 Main calculation results

3.1 $PbTiO_3$ and $SrTiO_3$ main bulk properties As a starting point of our B3PW calculations, we calculated main characteristics of the perfect $PbTiO_3$ and $SrTiO_3$ bulk, in order to compare later obtained results with those of $PbTiO_3/SrTiO_3$ (001) heterostructures. Our calculated, by means of hybrid B3PW exchange-correlation functional, bulk lattice constant for $PbTiO_3$ (3.93 Å) is only by 0.76% smaller than the experimental $PbTiO_3$ lattice constant of 3.96 Å [50]. In contrast, our calculated $SrTiO_3$ bulk lattice constant (3.90 Å) is almost in a perfect agreement with the experimental value (3.89 Å) [51]. Our B3PW calculated band gap for the $PbTiO_3$ perovskite at the Γ-point (4.32 eV) is by 17.71% overestimated with respect to the experimental value of (3.67 eV) [50]. Again, for $SrTiO_3$ perovskite, almost perfect agreement between both the calculated (3.63 eV) and experimentally measured (3.75 eV) [52] band gaps are observed.

Our B3PW calculated effective atomic charges for $PbTiO_3$ and $SrTiO_3$ perovskites, using Mulliken bond population analysis, are considerably smaller than their perfect ionic values of +2*e*, +4*e* and -2*e*, respectively. Calculated numerical values for $PbTiO_3$ effective charges are equal to (+1.35*e*, +2.34*e* and -1.23*e*, respectively). Also for $SrTiO_3$ perovskite, our calculated effective atomic charges (+1.87*e*, +2.35*e* and -1.41*e*, respectively), are considerably smaller than the classical ionic charges. The population of the chemical bond between Ti and O atoms is +0.098*e* in $PbTiO_3$, and slightly smaller (+0.088*e*) in $SrTiO_3$. The chemical bond populations calculated between Pb and O atoms in $PbTiO_3$ (+0.016*e*) and between Sr and O atoms in $SrTiO_3$ (-0.010*e*) are much smaller.

3.2 $SrTiO_3/PbTiO_3$ (001) heterostructures Our *ab initio* B3PW calculations dealing with $PbTiO_3/SrTiO_3$ (001) heterostructures have been performed using the $SrTiO_3$ (001) substrate consisting of eleven alternating TiO_2 or SrO atomic layers in the (001) direction symmetrically terminated from both sides by TiO_2 layers. Afterwards, we modelled $PbTiO_3$ epitaxial growth by adding a pair of $PbTiO_3$ (001) monolayers symmetrically to both sides of TiO_2-terminated $SrTiO_3$ (001) substrate. Thereby, we performed our B3PW calculations for ten different $PbTiO_3$ (001) film concentrations, ranging from one monolayer, symmetrically augmented to $SrTiO_3$ (001) substrate from both sides, up to 10 $PbTiO_3$ (001) film monolayers added symmetrically to both sides of $SrTiO_3$ (001) substrate. Owing to the constraints forced by the system symmetry, in our B3PW calculations positions of all atoms were relaxed only along the z-axis, the same as in our recent pilot studies dealing with $BaTiO_3/SrTiO_3$ [53] and $PbZrO_3/SrZrO_3$ [54] (001) interfaces. Thereby, due to the symmetry restrictions, we do not include in our B3PW calculations the possible oxygen rotations in the x, y plane, as often discussed in the literature [37, 55, 56].

In our B3PW calculations atomic shifts Δz along the z axis were simulated in comparison to the averaged z position of the former layer, as described in Eq. (1), in order to avoid a permanent increase of their value. All our B3PW calculated atomic displacements are inside 8.54% of the lattice constant. All upper layer atoms (Δz) of on the $SrTiO_3$ (001) substrate augmented $PbTiO_3$ (001) thin film strongly relax inwards. Magnitude of inward relaxation Δz strongly depends on the number of augmented layers and always exceeds 6% from the lattice constant: -6.01 (1 layer), -7.76 (2 layers), -6.97 (3 layers), -8.25 (4 layers), -7.26 (5 layers), -8.38 (6 layers), -7.34 (7 layers), -8.54 (8 layers), -7.42 (9 layers), -8.54 (10 layers). It is worth to notice, that surface upper layer atom relaxations Δz of the PbO-terminated augmented $PbTiO_3$ (001) thin film, *i.e.*, -6.01 (1); -6.97 (3); -7.26 (5); -7.34 (7) and -7.42 (9) are always smaller than those of the TiO_2-terminated augmented $PbTiO_3$ (001) thin film: -7.76 (2); -8.25 (4); -8.38 (6); -8.54 (8) and -8.54 (10). For both PbO and TiO_2-terminations of $PbTiO_3$ (001) thin film, the magnitude of atomic relaxation Δz increases as a function of the number of augmented layers. For both PbO and TiO_2-terminations of augmented $PbTiO_3$ (001) thin film, all upper layer atoms are displaced inwards (Δz), towards the bulk, all second layer atoms (Δz) relax outwards, all third layer atoms again relax inwards, while all fourth layer atoms are shifted outwards. This tendency is true even for fifth and sixth layer atoms of both PbO and TiO_2-terminated augmented $PbTiO_3$ (001) thin films, the former relax inwards, while the latter outwards.

As a consequences of the large contribution of the covalency in Ti-O bonds, our B3PW calculated Mulliken charges of Ti and O are quite different from Ti and O formal ionic charges of +4*e* and -2*e*, respectively. As follows from our previous studies, the Ti-O chemical bonds near TiO_2-terminated (001) surfaces of both $PbTiO_3$ and $SrTiO_3$ slabs increase their covalency as compared to that of Ti-O chemical bond in bulk $PbTiO_3$ and $SrTiO_3$ perovskites

[29]. According to performed B3PW calculations, the increase of the Ti-O chemical bond covalency (0.158*e*) in comparison with the $PbTiO_3$ bulk (0.098*e*), is observed also near the $PbTiO_3/SrTiO_3$ (001) interface. The augmented $PbTiO_3$ (001) thin film upper layer TiO_2-terminated planes, independently from the number of augmented layers, 2, 4, 6, 8 or 10 layers, always attracts exactly 0.08*e*. At the same time, the PbO-terminated $PbTiO_3/SrTiO_3$ (001) heterostructures becomes more positive: +0.13*e* for 1 augmented $PbTiO_3$ layer, +0.14*e* (3 layers), +0.14*e* (5 layers), +0.15*e* (7 layers) and +0.15*e* (9 layers). The largest positive monolayer charge (+0.15*e*) is observed for PbO-terminated 7 and 9 layer thick augmented $PbTiO_3$ (001) thin film upper layers. In contrast, the largest negative monolayer charge (-0.17*e*) is observed for 7 and 9 layer thick augmented $PbTiO_3$ (001) thin film Ti and two O atoms containing upper sublayer. It is interesting to notice, that for each monolayer of the $SrTiO_3$ (001) substrate, charge magnitudes always are more than several times larger, than the augmented $PbTiO_3$ (001) thin film each monolayer charges. For example, the central $SrTiO_3$ (001) substrate layer Sr and O summary charges varies from +0.45*e* till +0.47*e*, but the first substrate layer charges containing Ti and two O atoms varies from -0.44*e* till -0.47*e*. Also the second, third and fourth $SrTiO_3$ (001) substrate monolayer charges are almost the same as for the zero and first monolayers. Nevertheless, it is interesting to notice, that for the fifth, and simultaneously the upper $SrTiO_3$ (001) monolayer, the Mulliken charges are quite different, than that for the other substrate monolayers. They are in the range from -0.28*e* till -0.31*e*, and thereby they are approximately in the middle between the other $SrTiO_3$ (001) substrate monolayer charges, as well as the augmented $PbTiO_3$ (001) thin film all monolayer charges.

Figure 2 analyzes the electronic charge density redistribution, which happens at the $PbTiO_3/SrTiO_3$ (001) heterostructure, in comparison to the pure $SrTiO_3$ and $PbTiO_3$ (001) slabs. By definition, the charge density redistribution is the electron density at the (001) interface minus the sum of electron densities in separately isolated $SrTiO_3$ (001) substrate and $PbTiO_3$ (001) thin film slabs and is plotted in Fig. 2 for both 3- and 4-UC thick $PbTiO_3/SrTiO_3$ (001) heterostructures. Figure 2 demonstrate, that the most important distortions happens at the (001) interface due to the compensation of the surface effects of the slabs. Plots also demonstrate that the electronic structure of the (001) substrate of non-stoichiometric heterostructures is distorted similarly to that of stoichiometric ones. The situation in the (001) thin films is just opposite.

Our B3PW calculated density of states (DOS) projected layer by layer onto all orbitals of Pb, Sr, Ti and O atoms of three and four unit cell (UC) thick $PbTiO_3/SrTiO_3$ (001) heterostructures are plotted in Figs. 3 and 4. The same as for all bulk ABO_3 perovskites [21, 29, 57-60], the top of valence band for $PbTiO_3/SrTiO_3$ (001) heterostructure consists mainly of O(2*p*) orbitals. At the same time, the bottom of the conduction band for $PbTiO_3/SrTiO_3$ (001) heterostructures is formed mostly from Ti(3*d*) atomic orbitals.

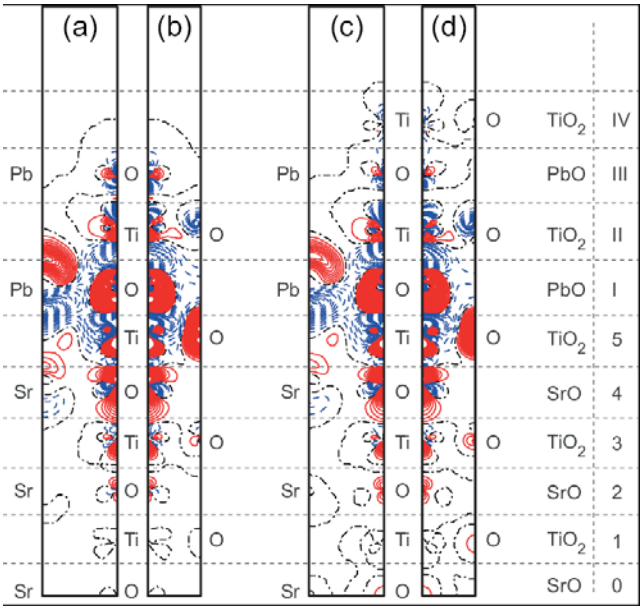

Figure 2 Our B3PW calculated difference electron charge density maps for $PbTiO_3/SrTiO_3$ (001) interfaces: (a) (110) cross-section for N_{PbTiO3} = 3, (b) (100) cross-section for N_{PbTiO3} = 3, (c) (110) cross-section for N_{PbTiO3} = 4, (d) (100) cross-section for N_{PbTiO3} = 4. Red solid, blue dashed and black dash-dotted isolines represent positive, negative and zero values of the difference charge density, respectively. Isodensity curves are drawn from -0.025 to +0.025 *e* $Å^{-3}$ with an increment of 0.0005 *e* $Å^{-3}$. Right-side bar shows the atomic monolayers from which atoms are originated. $SrTiO_3$ and $PbTiO_3$ monolayers are numbered beginning from the center of the slab. Planes (monolayers) are numbered separately for $SrTiO_3$ (001) substrate as well as for $PbTiO_3$ (001) nanofilm with Arabic and Roman numbers.

Our B3PW calculated band gaps of 4.32 eV for the $PbTiO_3$ perovskite bulk and 3.63 eV for the $SrTiO_3$ perovskite bulk are in a fair agreement with experimental results of 3.67 and 3.75 eV, respectively. The B3PW calculated band gap for TiO_2-terminated eleven layer containing $SrTiO_3$ (001) substrate is considerably reduced with respect to the $SrTiO_3$ bulk band gap and is equal to 2.58 eV. The B3PW calculated band gap for the PbO-terminated $PbTiO_3$ (001) thin augmented on the $SrTiO_3$ (001) substrate containing one layer is equal to 3.45 eV (Fig. 5). The band gaps for PbO-terminated augmented (001) thin films containing 3, 5, 7 and 9 layers are equal to 3.25, 3.08, 2.99 and 2.94 eV, respectively. The B3PW calculated band gaps for the TiO_2-terminated augmented $PbTiO_3$ (001) thin film on the $SrTiO_3$ (001) substrate containing 2, 4, 6, 8 and 10 layers are equal to 3.18, 3.17, 3.05, 2.99 and 2.93 eV, respectively.

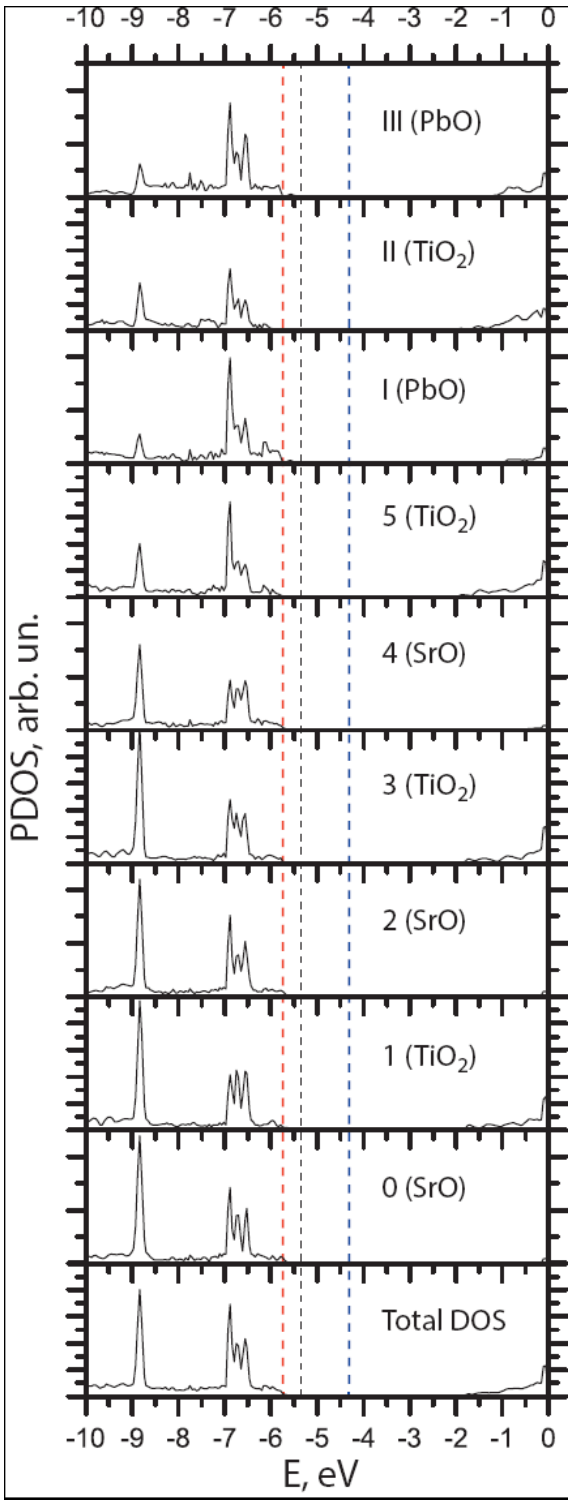

Figure 3 By means of the B3PW hybrid exchange-correlation functional calculated layer by layer projected density of states of three UC thick $PbTiO_3/SrTiO_3$ (001) heterostructure. Energy scale is plotted regarding the vacuum level.

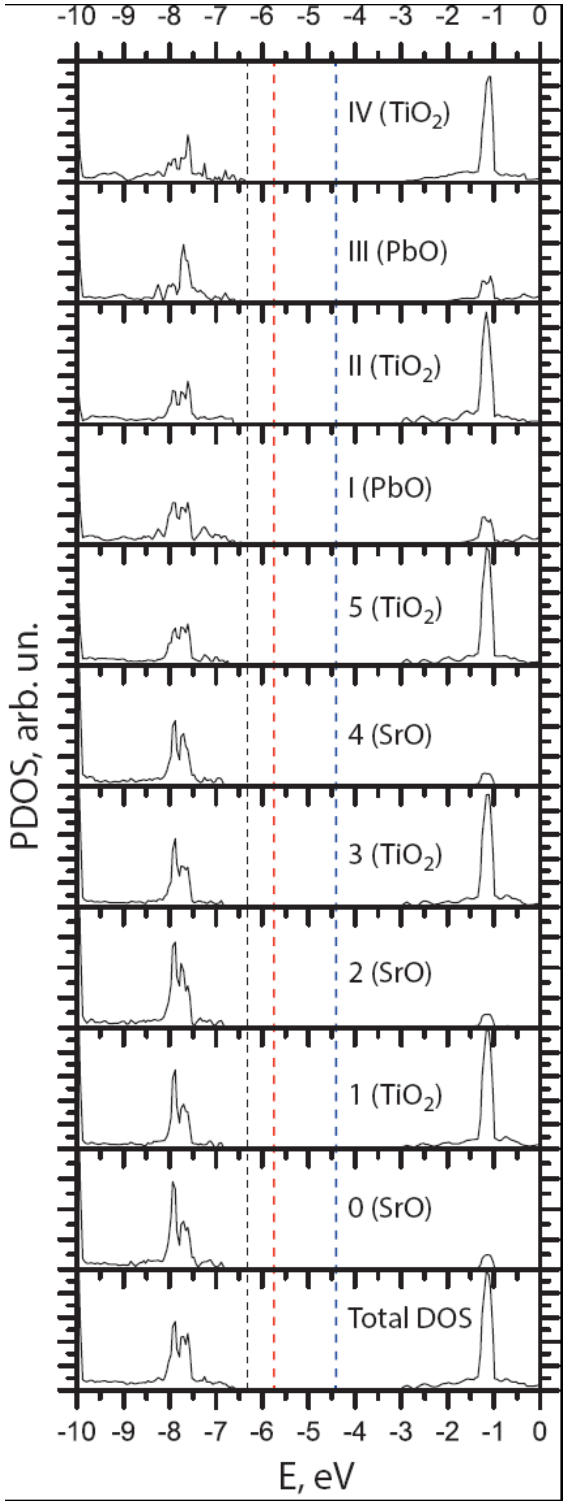

Figure 4 By means of the B3PW hybrid exchange-correlation functional calculated layer by layer projected density of states of four UC thick $PbTiO_3/SrTiO_3$ (001) heterostructure. Energy scale is plotted regarding the vacuum level.

3.3 Suitability of $PbTiO_3/SrTiO_3$ (001) heterostructures for photocatalysis Dissociation of H_2O molecules under the influence of solar light on semiconductor electrode is very promising process for production of hydrogen fuel, which is environmentally friendly energy source [61]. 2D interfaces inside perovskite $PbTiO_3/SrTiO_3$ (001) heterostructures have been checked as materials potentially suitable for photocatalytic applications. Their efficiency depends on relative position of the band gap edges (the visible light interval between infrared and ultraviolet ranges of electromagnetic spectrum corresponds to gap widths 1.5–2.8 eV) accompanied by a proper alignment of valence and conduction bands ($\mathcal{E}_{VB}$ and $\mathcal{E}_{CB}$) as well as occupied and unoccupied induced levels ($\mathcal{E}_{HOIL}$ and $\mathcal{E}_{LUIL}$) relative to both reduction (H^+/H_2) and oxidation (O_2/H_2O) potentials (-4.44 eV and -5.67 eV, respectively). They must be positioned inside the band gap as shown in our recent papers describing suitability for photocatalysis of $SrTiO_3$ nanotubes [62] and nanonwires [63], respectively:

$$\mathcal{E}_{VB} < \mathcal{E}_{HOIL} < \mathcal{E}_{O2/H2O} < \mathcal{E}_{LUIL} < \mathcal{E}_{CB}. \quad (2)$$

As follows from Figs. 3 and 4 containing redox levels $\mathcal{E}_{O2/H2O}$ and $\mathcal{E}_{H+/H2}$ inserted in DOSs plots, $PbTiO_3/SrTiO_3$ (001) heterostructures containing 4 UC-thick $PbTiO_3$ (001) nanofilm can be considered as potential candidates for photocatalytic applications, while 3 UC-thick film not since conditions of Eq. (2) are not fulfilled in the latter case (because the top of its valence band $\mathcal{E}_{VB}$ overlaps with $\mathcal{E}_{O2/H2O}$ level which leads to recombination between electron excited by photon absorption and remaining hole). However, the band gap of heterostructure containing 4 UC-thick nanofilm (~3.4 eV) corresponds to ultraviolet light range, being too wide for sunlight energy conversion (15-17%). The next step of possible $PbTiO_3/SrTiO_3$ (001) heterostructure adaptation as photoelectrode would be its doping, presumably by non-metal atoms substituted regular oxygens [62].

4 Conclusions We have performed *ab initio* B3PW calculations on a number of $PbTiO_3/SrTiO_3$ (001) heterostructures. For the TiO_2-terminated $PbTiO_3/SrTiO_3$ (001) heterostructure upper layer, the Ti-O chemical bond population is 0.158*e*, which is approximately 1.6 times larger than the respective Ti-O chemical bond population 0.098*e* in the $PbTiO_3$ perovskite bulk.

For both PbO and TiO_2-terminations of the $PbTiO_3$ (001) thin film, augmented on the $SrTiO_3$ (001) substrate, the magnitudes of atomic Δz relaxations increase as functions of the number of augmented monolayers. For both PbO and TiO_2-terminations all upper, third and fifth monolayers are displaced inwards (Δz is negative), whereas all second, fourth and sixth monolayers are displaced outwards (Δz is positive).

The B3PW calculated $PbTiO_3/SrTiO_3$ (001) heterostructure band gaps, independently from the number of augmented layers, are always smaller than the $PbTiO_3$ and $SrTiO_3$ bulk band gaps. For both PbO and TiO_2-terminated $PbTiO_3/SrTiO_3$ (001) heterostructures, their band gaps are reduced due to the increased number of $PbTiO_3$ (001) monolayers. It is worth to notice, that according to previous B3PW calculations [53, 54] dealing with $BaTiO_3/SrTiO_3$ and $PbZrO_3/SrZrO_3$ (001) interfaces (Fig. 5), the calculated band gaps for AO-terminated augmented (001) thin films always were considerably larger than the band gaps for augmented BO_2-terminated (001) films independently from the number of layers. In contrast, for the case of $PbTiO_3/SrTiO_3$ (001) interfaces, situation is slightly different, since for both, 7-layer PbO-terminated and 8-layer TiO_2-terminated augmented $PbTiO_3$ (001) thin films, their band gaps are equal to 2.99 eV.

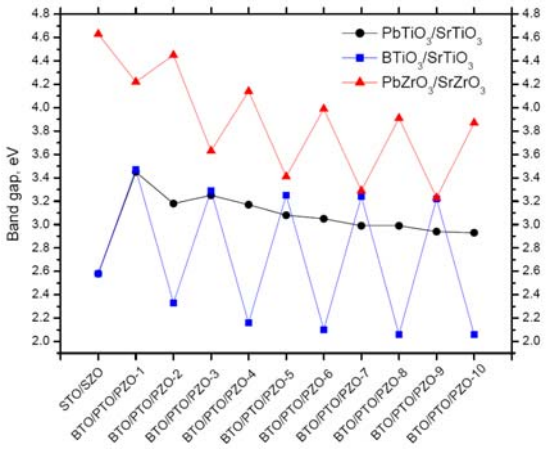

Figure 5 Our B3PW calculated optical band gaps for $PbTiO_3/SrTiO_3$ (001) heterostructures. The number of deposited $PbTiO_3$ monolayers are changed from 0 (corresponds to TiO_2-terminated $SrTiO_3$ (001) substrate till 10. Dashed lines are used for better perception. B3PW calculated band gaps for $BaTiO_3/SrTiO_3$ and $PbZrO_3/SrZrO_3$ (001) interfaces [58, 59] are listed for comparison purposes.

It is worth to notice, that for each monolayer of the $SrTiO_3$ (001) substrate, charge magnitudes always are more than several times larger, than for each monolayer of the augmented $PbTiO_3$ (001) thin film. For example, the central $SrTiO_3$ (001) substrate layer Sr and O summary charges varies from +0.45*e* till +0.47*e*. It is interesting to notice, that for the fifth, and simultaneously the upper $SrTiO_3$ (001) monolayer, the Mulliken charges are quite different, as compared to other substrate monolayers. They are in the range from -0.28*e* till -0.31*e*, and thereby they approximately correspond to the averaged value between another $SrTiO_3$ (001) substrate monolayer charges, as well as all monolayer charges of the augmented $PbTiO_3$ (001) thin film. Along with the performed Mulliken charge analysis, also Fig. 2 confirms, that the most important distortions happens at the (001) interface, due to the compensation of the surface effects of the slabs.

$PbTiO_3/SrTiO_3$ (001) heterostructures with even number of layers inside $PbTiO_3$ nanonthin films, according to our predictions, can be directly suitable for photocatalytic applications after their doping by non-metal atoms substituted regular oxygens (e.g., N_O and S_O mono-dopants as well as N_O+S_O co-dopant).

Acknowledgements The presented study has been supported by the Latvian Council of Science Grant No. 374/2012, as well as the EC project WATERSPLIT (ERA.Net.RUS Plus Grant No. 237). The authors are grateful to E. A. Kotomin for many stimulating discussions.

References

[1] L. Kronik and Y. Shapira, Surf. Sci. Rep. **37**, 1 (1999).
[2] R. C. Cammarata, Prog. Surf. Sci. **46**, 1 (1994).
[3] M. Causa, R. Dovesi, E. Kotomin, and C. Pisani, J. Phys. C **20**, 4983 (1987).
[4] E. Kotomin, A. Shluger, M. Causa, R. Dovesi, and F. Ricca, Surf. Sci. **232**, 399 (1990).
[5] D. Ochs, M. Brause, S. Krischok, P. Stracke, W. Maus-Friedricks, V. Puchin, A. Popov, and V. Kempter, J. Electron. Spectrosc. Relat. Phenom. **88**, 725 (1998).
[6] A. Postawa, J. Kolodziej, G. Baran, P. Czuba, P. Piatkowski, M. Szymonski, I. Plavina, and A. Popov, Nucl. Instrum. Methods B **100**, 228 (1995).
[7] V. N. Kuzovkov, A. I. Popov, E. A. Kotomin, M. A. Monge, R. Gonzalez, and Y. Chen, Phys. Rev. B **64**, 064102 (2001).
[8] O. I. Aksimentyeva, V. P. Savchyn, V. P. Dyakonov, S. Piechota, Y. Y. Horbenko, I. Y. Opainych, P. Y. Demchenko, A. Popov, and H. Szymchak, Mol. Cryst. Liq. Cryst. **590**, 35 (2014).
[9] V. P. Savchyn, A. I. Popov, O. I. Aksimentyeva, H. Klym, Yu. Yu. Horbenko, V. Serga, A. Moskina, and I. Karbovnyk, Low. Temp. Phys. **42**, 760 (2016).
[10] N. Erdman, K. R. Poeppelmeier, M. Asta, O. Warschkov, D. E. Ellis, and L. D. Marks, Nature **419**, 55 (2002).
[11] R. I. Eglitis and D. Vanderbilt, Phys. Rev. B **77**, 195408 (2008).
[12] R. A. Evarestov, A. V. Bandura, and V. E. Alexandrov, Phys. Status Solidi B **243**, 2756 (2006).
[13] G. Borstel, R. I. Eglitis, E. A. Kotomin, and E. Heifets, Phys. Status Solidi **236**, 253 (2003).
[14] Z. Q. Li, J. L. Zhu, C. Q. Wu, Z. Tang, and Y. Kawazoe, Phys. Rev. B **58**, 8075 (1998).
[15] D. M. Kienzle, A. E. Becerra-Toled,o and L. D. Marks, Phys. Rev. Lett. **106**, 176102 (2011).
[16] C. Cheng, K. Kunc, and M. H. Lee, Phys. Rev. B **62**, 10409 (2000).
[17] R. Herger, P. R. Willmott, O. Bunk, C. M. Schlepütz, B. D. Patterson, and B. Delley, Phys. Rev. Lett. **98**, 076102 (2007).
[18] M. Fechner, S. Ostanin, and I. Mertig, Phys. Rev. B **77**, 094112 (2008).
[19] E. A. Kotomin, R. I. Eglitis, J. Maier, and E. Heifets, Thin Solid Films **400**, 76 (2001).
[20] A. Munkholm, S. K. Streiffer, M. V. Ramana Murty, J. A. Eastman, C. Thompson, O. Auciello, L. Thompson, J. F. Moore, and G. B. Stephenson, Phys. Rev. Lett. **88**, 016101 (2001).
[21] S. Piskunov, E. A. Kotomin, E. Heifets, J. Maier, R. I. Eglitis, and G. Borstel, Surf. Sci. **575**, 75 (2005).
[22] Z. Jiang, R. Zhang, D. Wang, D. Sichuga, C. L. Jia, and L. Bellaiche, Phys. Rev. B **89**, 214113 (2014).
[23] J. M. Zhang, Q. Pang, K. W. Xu, and V. Ji, Surf. Interface Anal. **40**, 1382 (2008).
[24] A. M. Kolpak, N. Sai, and A. M. Rappe, Phys. Rev. B **74**, 054112 (2006).
[25] R. I. Eglitis and D. Vanderbilt, Phys. Rev. B **76**, 155439 (2007).
[26] T. Shimada, S. Tomoda, and T. Kitamura, J. Phys.: Condens. Matter **22**, 355901 (2010).
[27] T. Xu, T. Shimada, Y. Araki, J. Wang, and T. Kitamura, Nano Lett. **16**, 454 (2016).
[28] B. K. Mani, C. M. Chang, S. Lisenkov, and I. Ponomareva, Phys. Rev. Lett. **115**, 097601 (2015).
[29] R. I. Eglitis, Int. J. Mod. Phys. B **28**, 1430009 (2014).
[30] Y. B. Xue, D. Chen, Y. J. Wang, Y. L. Tang, Y. L. Zhu, and X. L. Ma, Philos. Mag. **95**, 2067 (2015).
[31] R. Schafranek, S. Li, F. Chen, W. Wu and A. Klein, Phys. Rev. B **84**, 045317 (2011).
[32] M. Dawber, C. Lichtensteiger, M. Cantoni, M. Veithen, P. Ghosez, K. Johnston, K. M. Rabe, and J. M. Triscone, Phys. Rev. Lett. **95**, 177601 (2005).
[33] T. Kiguchi, K. Aoyagi, Y. Ehara, H. Funakubo, T. Yamada, N. Usami, and T. J. Konno, Sci. Technol. Adv. Mater. **12**, 034413 (2011).
[34] P. Zubko, N. Stucki, C. Lichtensteiger, and J. M. Triscone, Phys. Rev. Lett. **104**, 187601 (2010).
[35] Y. Zheng and C. H. Woo, Appl. Phys. A **97**, 617 (2009).
[36] Z. Y. Zhu, B. Wang, H. Wang, Y. Zheng, and Q. K. Li, Chin. Phys. **16**, 1780 (2007).
[37] A. K. Yadav, C. T. Nelson, S. L. Hsu, Z. Hong, J. D. Clarkson, C. M. Schlepütz, A. R. Damodaran, P. Shafer, E. Arenholz, L. R. Dedon, D. Chen, A. Wishwanath, A. M. Minor, L. Q. Chen, J. F. Scott, L. W. Martinand, and R. Ramesh, Nature **530**, 198 (2016).
[38] P. Aguado-Puente, and J. Junquera, Phys. Rev. B **85**, 184105 (2012).
[39] M. Dawber, K. M. Rabe, and J. F. Scott, Rev. Mod. Phys. **77**, 1083 (2005).
[40] A. J. Moulson and J. M. Herbert, Electroceramics, 2nd ed. (Wiley, New York, 2003).
[41] R. E. Cohen, Nature **358**, 136 (1992).
[42] R. Dovesi, V. R. Saunders, C. Roetti, R. Orlando, C. M. Zicovich-Wilson, F. Pascale, B. Civalleri, K. Doll, N. M. Harrison, I. J. Bush, Ph. D'Arco, and M. Llunell, CRYSTAL09 User's Manual, University of Torino, Torino, Italy, 2009.
[43] S. Piskunov, E. Heifets, R. I. Eglitis, and G. Borstel, Comput. Mater. Sci. **29**, 165 (2004).
[44] A. D. Becke, J. Chem. Phys. **98**, 5648 (1993).
[45] R. S. Mulliken, J. Chem. Phys. **23**, 1833 (1955).
[46] R. S. Mulliken, J. Chem. Phys. **23**, 184 (1955).
[47] R. S. Mulliken, J. Chem. Phys. **23**, 2338 (1955).
[48] R. S. Mulliken, J. Chem. Phys. **23**, 2343 (1955).
[49] H. J. Monkhorst and J. D. Pack, Phys. Rev. B **13**, 5188 (1976).

[50] V. Železný, D. Chvostová, D. Šimek, F. Máca, J. Mašek, N. Setter, and Y. H. Huang, J. Phys.: Condens. Matter **28**, 025501 (2016).
[51] K. H. Hellwege and A. M. Hellwege (Eds.), Ferroelectrics and Related Substances, New Series, Vol. 3, Landolt-Börnstein (Springer-Verlag, Berlin, 1969).
[52] K. van Benthem, C. Elsasser, and R. H. French, J. Appl. Phys. **90**, 6156 (2001).
[53] S. Piskunov and R. I. Eglitis, Solid State Ion. **274**, 29 (2015).
[54] S. Piskunov and R. I. Eglitis, Nucl. Instrum. Methods Phys. Res. B **374**, 20 (2016).
[55] A. Vailionis, H. Boschker, W. Siemons, E. P. Houwman, D. H. A. Blank, G. Rijnders, and G. Koster, Phys. Rev. B **83**, 064101 (2011).
[56] K. D. Fredrickson and A. A. Demkov, Phys. Rev. B **91**, 115126 (2015).
[57] R. I. Eglitis, A. V. Postnikov, and G. Borstel, Phys. Rev. B **54**, 2421 (1996).
[58] A. V. Postnikov, T. Neumann, G. Borstel, and M. Methfessel, Phys. Rev. B **48**, 5910 (1993).
[59] R. I. Eglitis and S. Piskunov, Comp. Condens. Matter **7**, 1 (2016).
[60] R. I. Eglitis, Phys. Status Solidi B **252**, 635 (2015).
[61] A. Kudo and Y. Miseki, Chem. Soc. Rev. **38**, 253 (2009).
[62] S. Piskunov, O. Lisovski, J. Begens, D. Bocharov, Yu. F. Zhukovskii, M. Wessel, and E. Spohr, J. Phys. Chem. C **119**, 18686 (2015).
[63] A. V. Bandura, R. A. Evarestov, and Yu. F. Zhukovskii, Royal Chem. Soc. Adv. **5**, 24115 (2015).

